 doi:10.20944/preprints202007.0072.v1

Article

A Rapid Extraction Method of Regional Scale Agricultural Disasters Based on Google Earth Engine

Zhengrong Liu [1], Huanjun Liu [1,2], Chong Luo [2], Haoxuan Yang [3], Yongchol Ju [4], Dong Guo [2,*]

[1] School of Pubilc Adminstration and Law, Northeast Agricultural University, Harbin 150030, P.R.China; liuzhengronghxs@163.com(Z.L.); huanjunliu@yeah.net(H.L.)

[2] Northeast Institute of Geography and Agroecology Chinese Academy of Sciences, Changchun 130102, China; luochong93@yeah.net

[3] College of Surveying and Geo-Informatics, Tongji University, 1239 Siping Road, Shanghai 200092, China; yhx965665334@163.com

[4] Wonsan University of Agriculture, Won san city, Kangwon Province; 1627504243@163.com

* Correspondence: guodong@iga.ac.cn; Tel.: +86-1874-519-4393 (F.L.)

Abstract: Remote sensing has been used as an important tool for disaster monitoring and disaster scope extraction, especially for the analysis of temporal and spatial disasters patterns of large-scale long time series. In order to find out a rapid and effective method to monitor disaster in a wide range, based on the Google Earth Engine cloud platform, this study used MODIS vegetation index products of 250 meter spatial resolution synthesized in 16 days during the year 2005-2019 and three kinds of disaster monitoring and scope extraction models are proposed: normalized vegetation index median time standardization ($R_{NDVI\_TM(i)}$) model, the normalized vegetation index median phenology Standardization($R_{NDVI\_AM(i)(j)}$) model, normalized vegetation index median spatiotemporal Standardization ($R_{NDVI\_ZM(i)(j)}$) model. The optimal threshold of disaster extraction for each model in different time phases was determined by Otsu method, and the extraction results were verified by Medium resolution image and ground measured data of the same or quasi-same period. Finally, the disaster scope of cultivated land in Heilongjiang province from 2010 to 2019 was extracted and the temporal and spatial pattern of disasters was analyzed based on the meteorological data. It shows that the three above-mentioned models have high disaster monitoring and range extraction capabilities with the verification accuracy of $R_{NDVI\_TM(i)}$ 97.46%, $R_{NDVI\_AM(i)(j)}$ 96.90%, and $R_{NDVI\_ZM(i)(j)}$ 96.67% respectively. The spatial and temporal distribution of disasters is consistent with the disaster of the insured plots and meteorological data in the whole province. Meanwhile, it turns out that different monitoring and extraction methods are used in different disasters, among which wind hazard and insect disasters often need to be delayed for 16 days to observe. Each model also has various sensitivity and applicability to different disasters. Compared with other methods, this method is fast, and convenient, which allows it to be used for large-scale agricultural disaster monitoring and is easy to be applied into other research areas. The research provides a new idea for large-scale agricultural disaster monitoring.

Keywords: Google Earth Engine; MODIS; Disaster monitoring

1. Introduction

Climate impact and environmental change are always important factors restricting the development of agricultural production. Among them, the impacts of drought, wind disaster, insect disaster, hailstorm and other agricultural disasters are the most significant. Under the trend of global warming, the increasing frequency and intensity of various extreme weather events in the world has brought great harm to food security and agricultural development [1]. The traditional agricultural disaster monitoring methods are mainly field investigation and sampling, which are hard to implement in large areas since they are time-consuming. Compared with those traditional methods, agricultural disaster remote sensing monitoring has the advantages of high space-time continuous access to surface information, fast data acquisition speed, wide range. Thus, remote sensing has been widely used in agricultural disaster and vegetation dynamic monitoring, and many remote sensing measurement methods have been developed to monitor global vegetation and extreme climate events [2,3]. Remote sensing monitoring of agricultural disaster takes an essential place in rapid crop loss assessment, crop condition monitoring, crop insurance and food security. Therefore, it is urgent to establish a rapid and large-scale agricultural disaster monitoring method with remote sensing as its technical support.

At present, many agricultural disaster monitoring methods are proposed, including ground spectral features, remote sensing vegetation index and vegetation index time series. Such as Normalized Vegetation Index (NDVI), Enhanced Vegetation Index(EVI), The Normalized Difference Water Index(NDWI), Vegetation Condition Index (VCI),Vegetation Health Index (VHI), Disaster Vegetation Damage Index (DVDI), Fire Weather Index(FWI), Crop Water Stress Index(CWSI), Vegetation Supply Water Index(VSWI), Temperature Vegetation Dryness Index(TVDI) and other vegetation indexes based on remote sensing parameters are widely used in disaster monitoring, and daily scale forest fires have been developed based on these indexes Hazard prediction system (FFDFS) for drought monitoring and fire risk assessment and remote sensing flood disaster crop loss assessment service system (RF-CLASS) for crop losses caused by floods [4,5,6,7,8,9,10].VCI has been proven to be an effective means of monitoring drought occurrence and measuring the intensity, duration and impact of droughts around the world. The spatial and temporal range of agricultural drought can be studied through VCI [11], but there is no high correlation between it and the meteorological drought index based on the weather station [12]. VCI is not very sensitive to short-term precipitation shortages. Meanwhile, there is also significant spatial variability in the relationship strength between VCI and meteorological drought index [13]. VHI is a widely used comprehensive remote sensing drought index, which aims to solve the limitations of VCI in areas with high soil moisture and long-term cloudy areas [14]. It is also used to evaluate the degree of agricultural drought and extract the spatial and temporal range of drought [15]. However, drought monitoring through VHI needs to assume a negative correlation between NDVI and LST. Therefore, VHI is not applicable to regions and periods where the NDVI-Ts correlation coefficient is non-negative [16]. TVDI is feasible for large-scale drought monitoring, but TVDI is usually affected by its high sensitivity to clouds, so it should not be used to monitor moderate and severe droughts [17][18][19]. Crop Water Stress Index (CWSI) is widely used as an indicator of crop water status. The short-term oscillations of canopy temperature and vegetative flushing are the main factors that cause the limitation of CWSI. CWSI is less effective in wet areas [20][21]. VSWI and TVDI can be used for drought monitoring, but they are not suitable for areas with large elevation changes [22]. At the same time, CWSI, TVDI and VSWI have a certain lag in drought detection, and it will take some time to respond [23]. In view of the limitation of lagging vegetation index, hyperspectral remote sensing technology can be used to monitor winter wheat freezing injury and locust disaster [24][25][26]. DVDI has a linear relationship with crop yield reduction, which is often used in flood disaster and wind disaster monitoring, and an effective indicator of vegetation damage degree [27][28]. At the same time, EVI is also widely used to describe vegetation patterns in ecosystems affected by various hurricanes, such as tropical rain forests, tropical arid forests, and temperate arid grasslands. NDVI and EVI, as the most widely used remote sensing indicators, are usually used for crop growth monitoring. MODIS NDVI time series can be used to analyze the spatiotemporal evolution of droughts and ENSO events to estimate the yield loss caused by droughts [29][30][31]. In areas with less vegetation, the method based on vegetation index has limitations. In areas with less vegetation, the method based on vegetation index

has limitations. For desert locusts, based on Mir, NIR and red reflectance, multi temporal and multi spectral image analysis can effectively solve this problem [32].The corn fields damaged by hail can be effectively identified by comparing the ΔNDVI images before and after the hail of the HJ-1 CCD, but it is difficult to finely classify the damage [33][34]. Pixel-based time series based on Enhanced Vegetation Index (EVI) data can be extracted to detect flood disturbances to crop production, but when assessing flood events that occur during crop maturity, the accuracy rate is very low[35]. At the same time, the habitat of Asian locusts can be monitored [36]. There are studies using three different remote sensing green indexes, namely Normalized Vegetation Index (NDVI), Enhanced Vegetation Index (EVI) and Green Index (GI), to study the damage of frost to the canopy [37]. The above indicators have been widely used in crop growth monitoring in regions, countries and the world. Crop growth monitoring usually uses the normalized vegetation index (NDVI) as the main indicator of crop conditions. By combining the NDVI value with other variables for analysis and utilization. By calculating the difference between the multi-year average (or selected "reference" year) and the NDVI of that year to monitor the growth of crops [38]. However, this method has limitations: it requires a crop that is constant for many years, The average value, that is, the planting structure and distribution of the crop cannot be changed; or the error of the crop growth fluctuation selected as the reference year will affect the assessment results of this year. In order to avoid the change of the crop distribution and lead to information errors, Li C proposed a Monitoring the growth of winter wheat based on the percentage of crop NDVI (pNDVI) [39]; However, few studies can eliminate this limitation from the perspective of phenology. In addition, studies are mostly concentrated in smaller areas. For example, in terms of ground spectral characteristics monitoring disasters: the use of visible and near-infrared reflectance spectroscopy (VNIRS) is an alternative method for monitoring soil contaminated by heavy metals. However, the study area tends to focus on the scale of city and county [40][41]. Through the above research, we found that the traditional disaster monitoring methods rely on the disaster data collected by the ground stations, so as to construct indicators based on the data, the amount of data obtained is limited and the data acquisition is difficult. And many disaster monitoring based on remote sensing have some limitations in application. Most disaster monitoring research methods are limited by large image data, mostly concentrated in small time scales or small research areas, and the speed is slow, lacking a fast with large-scale disaster discrimination methods. Therefore, it is difficult to quickly analyze the temporal and spatial pattern of disasters in a certain area. GEE can solve this problem well, that is, it can quickly carry out large-scale and long-range disaster monitoring in a long-term sequence, and analyze the spatial and temporal pattern of the designated area. Google Earth Engine is a cloud platform that stores and processes BP-level global time series satellite images and vector data. Scholars from various countries have used it to conduct research in vegetation monitoring, land cover, agricultural applications, disaster management and earth science [42][43]. Beaton A et al. calculated the river's icebreaking period for flood monitoring on GEE [44]; Sazib N et al. verified the value of global soil moisture data for drought disaster monitoring using GEE [45]; Liu CC et al. developed a flood control and emergency system based on GEE (FPERS) [46]; Pradhan B et al. used GEE to provide physical support for the assessment of forest impacts of sand dune risk and hurricane in Sabha area [47]. Based on GEE, Lu L et al. studied the spatial characteristics of vegetation destruction induced by typhoons in coastal areas of southeastern China from 2000 to 2018 [48].

In the GEE, different vegetation indexes extracted through multi-temporal remote sensing images are used as standard values to reflect the normal conditions of crop growth in different regions and different growth stages, and compared with the vegetation index extracted in a single time phase to compare agricultural disasters in the region. The situation is monitored more accurately to make the results universally applicable. It is difficult to extract the standard value that can represent the average growth of crops. In this regard, this study introduces the normalized vegetation median time normalization ($R_{NDVI\_TM(i)}$) model, the normalized vegetation index median phenology standardization ($R_{NDVI\_AM(i)(j)}$) model, the normalized vegetation median time-space normalization ($R_{NDVI\_ZM(i)(j)}$) model, which comprehensively considers the effects of phenology, different disasters and crop types, and changes in planting structure, aims to propose a large-scale GEE-based monitoring method for rapid extraction of agricultural disasters. Attempt to use the MODIS 16-day NDVI time series data after

smooth reconstruction, compare and analyze the regional scale disaster index analysis map drawn by the three models; extract the disaster threshold of the study area through Otsu and compare it with HJ-1A/B CCD data Carry out validation and analyze the spatial and temporal distribution of disasters in Heilongjiang Province from 2000 to 2019. This method has good transplantability and can be quickly analyzed in other areas.

2. Materials and Methods

2.1 Study area

Located at 121°11 '-135°05' east longitude and 43°25 '-53°33' north latitude, Heilongjiang province crosses three humid zones from east to west. The total land area of the province is about 473,000 square kilometers, among which the agricultural land accounts for about 39.5045 million hectares. It is high in northwest, north and southeast, and low in northeast and southwest. Heilongjiang province is located in the west of the Pacific Ocean and the east of Eurasia, with a temperate continental climate. The average annual temperature in the province is mostly between -5 ℃ and 5 ℃, and the annual precipitation in the province is from 400 to 650mm, with uneven spatial and temporal distribution. Agricultural disasters are frequent, and the frequency of agricultural disasters represented by drought, flood, wind disaster, hailstorm, low temperature and freezing as well as disease and insect disasters increases [49][50].

2.2 Data

MOD13Q1

MODIS Vegetation Index (MOD13Q1) synthesized in 16 days with a 250m spatial resolution used in the research area is a terrestrial data product, which is fully known as MODIS/Terra Vegetation Indices 16-Day L3 Global 250m SIN Grid. This product is calculated by atmospheric correction of bidirectional surface reflectance. It possesses the advantages of medium spatial resolution, high temporal resolution, high spectral resolution, wide observation range and low cost.

HJ-1A/B

The verification data for disaster monitoring is HJ-1A/B data of environmental disaster mitigation satellite with a spatial resolution of 30m. The Chinese HJ-1A/B satellite makes synchronous ground observations, the CCD sensor captures the ground features of 30m pixel resolution at a minimum angle, and four bands cover Vis, visible light and near-infrared wavelength ranges. Each satellite has two CCD sensors; The constellation that consists of two satellites forms an observation network covering China and its surrounding areas, with large-scale, all-weather, all-day, dynamic environmental and disaster monitoring capabilities. At the same time, it is combined with the crop insurance plots from 2011 to 2019 to determine the disaster scope through visual interpretation. The personnel of the insurance company carried out field verification on 80% of the plots, and the accuracy turns out to be greater than 95%. It will be used as validation data of extracted extent of the disaster in this study.

Meteorological data

The spatial and temporal distribution characteristics of agricultural disasters in Heilongjiang province and its prefecture-level cities from 2010 to 2019 were analyzed based on the meteorological data of precipitation, temperature, humidity and sunshine duration inquired by Heilongjiang Provincial Bureau of Statistics (http://www.hlj.stats.gov.cn/) and China Meteorological Disaster Yearbook.

Cultivated land range data

In this paper, in order to avoid the influence of other land types and to conduct phenological zoning for the construction of disaster monitoring model, the disaster monitoring and extraction in the cultivated land was carried out using the land range extracted from the global 30 m land cover data.. The land use classification data refers to that from the Northeast Institute of Geography and Agro-Ecology of Chinese Academy of Sciences which used the land samples in 2014. Taking the CCD image of China Resources No. 1 satellite and Landsat remote sensing image as the main information sources, and adopting the manual visual interpretation method, we can obtain the cultivated land range as shown in Figure 1.

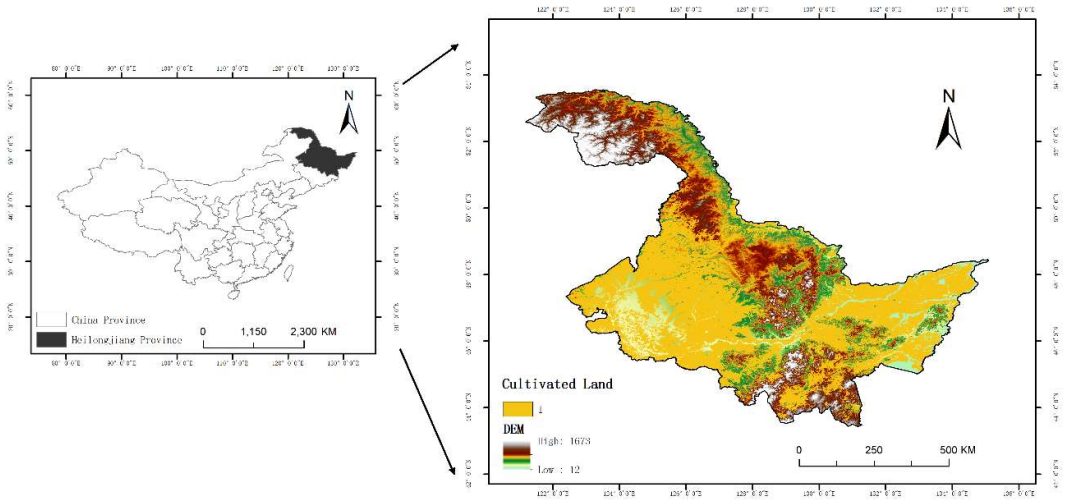

Figure 1. Cultivated land in Heilongjiang Province

2.3 Method

2.3.1 Data preprocessing

In this paper, MOD13Q1 reflectivity product is used to build the model on Google Earth Engine. GEE contains over 200 public data sets and over 5 million images, with an increase of approximately 4,000 images per day. Images captured into the Earth Engine are preprocessed. In GEE, MOD13Q1 NDVI products are calculated based on atmospheric corrected bidirectional surface reflectance, which is shielded against water, clouds, heavy aerosols and cloud shadows. We selected Good data and Marginal data from the SummaryQA to remove the impact of clouds and snow and ensure that the extracted disaster scope was not affected by outliers.

2.3.2 Phenological remote sensing zoning method

In terms of remote sensing image processing, 23 MODIS (MOD13Q1) remote sensing data with a spatial resolution of 250 m synthesized in 16 days in 2014 were emplyed to extract 11 crop phenological features, and the multi-phase NDVI time series was smoothly reconstructed by S-G filtering. The dynamic threshold method is used to extract the key phenological values, and the regions with similar phenological values are divided into one area for study, and multiscale segmentation is carried out within the cultivated land. Through this method, different crops with different geographical distribution and growth conditions can be divided into different agricultural phenological zones It is required that the laws of zonality and non-zonality of phenological distribution and the principle of

Preprints (www.preprints.org) | NOT PEER-REVIEWED | Posted: 5 July 2020 doi:10.20944/preprints202007.0072.v1

similarity and difference of crops be followed, and certain zoning method be adopted to divide a region into units of different grades with obvious difference in crop growth. Thus the province is divided into 39 phenological areas [51].

Table 1. Definition of phenological parameters in remote sensing

name	Definition interpretation
Start	crop growth initial period
End	End of crop growth
Amp	Amplitude
Base	Average of NDVI during Start and End
Length	Growth period length
Small	The integral of the average NDVI for the entire period
Max	NDVI maximum
Left	The slope between the 20% and 80% amplitude points on the left side of the rising curve
Right	The slope between the 20% and 80% amplitude over the right side of the descending curve
Mid	Midpoint of the whole period
Large	NDVI integral for the whole period

2.3.3 Construction of three disaster monitoring models

There are differences in phenological period and cultivated land planting structure in Heilongjiang Province, in vegetation indices of crops growing at the same time but in different areas, and in vegetation indices of different crops. Therefore, the results of disaster range recognition and extraction directly based on the difference of NDVI value of a certain phase are not precise and not universal. For this situation, the following three models are proposed and calculated in GEE:

$R_{NDVI\_TM(i)}$ model with normalized difference median vegetation index time:

$$R_{NDVI\_TM(i)} = \frac{NDVI_{TMED(i)} - NDVI_{TMED(i)}}{NDVI_{TMED(i)}} \times 100\% \quad (1)$$

In formula (1) : $R_{NDVI\_TM(i)}$ represents the time standardization value of NDVI(I) of the ith time phase in a certain year; NDVI(I) is the NDVI value of the ith time phase in a certain year; NDVITMED(I) is the NDVI value of the ith time phase for five consecutive years. The smaller the RNDVI_TM(I) value is, the worse the vegetation grows. Five years is chosen as the time scale, because the larger time scale is vulnerable to policy influences such as dryland diversion, crop rotation and change of planting structure. Meanwhile, the smaller time scale cannot reflect the time trend, and is susceptible to the influence of individual annual outliers.

Model of phenology standardization of the median value of normalized Difference vegetation index ($R_{NDVI\_AM(i)(j)}$) :

$$R_{NDVI\_AM(i)(j)} = \frac{NDVI_{(i)} - ND\_\_AMED(i)(j)}{NDVI_{AMED(i)(j)}} \times 100\% \quad (2)$$

In formula (2) : $R_{NDVI\_AM(i)(j)}$ is the phenological standardization value of the median value of $NDVI_{(i)}$ in the jth phenological region of the ith phase in a certain year, $NDVI_{(i)}$ is the NDVI value of the ith phase in a certain year, and $NDVI_{AMED(i)(j)}$ is the median value of the NDVI region in the jth phenological

region of the ith phase in a certain year. The smaller the $R_{NDVI\_AM(i)(j)}$ value is, the worse the vegetation grows.

$R_{NDVI\_ZM(i)(j)}$ model:

This method is an improvement on (3). Considering that the median value curve of NDVI region in the same phenological area in different years may be affected by the change of planting structure and other factors, so that the median value of NDVI extracted in different years at the same time can show great differences. Therefore, the regional median of the phase NDVI of phase I for five consecutive years is proposed as an alternative.

$$R_{NDVI\_ZM(i)(j)} = \frac{NDVI_{(i)} - NDVI_{ZMED(i)(j)}}{NDVI_{ZMED(i)(j)}} \times 100\% \quad (3)$$

In formula (3) : $R_{NDVI\_ZM(i)(j)}$ is the spatio-temporal standardization value of the median $NDVI_{(i)}$ of the jth phenological region of the ith phase in a certain year, $NDVI_{(i)}$ is the NDVI value of the ith phase in a certain year, and $NDVI_{ZMED(i)(j)}$ is the standardized median value of the NDVI of the jth phenological region of the ith phase for five consecutive years. The smaller $R_{NDVI\_ZM(i)(j)}$ value is, the worse the vegetation grows.

2.3.4 Determination of threshold value

Table 2. Phenological period of main crops in Heilongjiang Province

Crop Species	Crop Phenology （Ten days/Month）					
Rice	Sowing and Seedling Raising Mid-April-Mid-May	Transplanting and Rejuvenated Late-May-Early-June	Tillering Mid-June-Mid-July	Booting and Tasseling Late-July-Mid-August	Milk Late-August-Early-September	Mature Mid-September-Late-September
Corn	Seed and Emergence Late-April-Early-May	Seedling Mid-May-Mid-June	Jointing Late-June-Mid-July	Emasculation Late-July-Early-August	Milk Mid-August-Early-September	Mature Mid-September-Late-September
Soybean	Seed and Emergence Early-May-Late-May	Third Leaf Early-June-Late-June	Parabranching Late-June	Flowering Early-July-Mid-July	Podding Mid-August-Early-September	Mature Mid-September-Late-September

From mid-April to early June, crops in Heilongjiang province are in the seeding stage and seedling stage, during which the crop coverage is low and the NDVI value is small, easily susceptible to the soil background value. Therefore, this paper starts to extract the disaster scope from time phase DOY 177. In mid-September, precocity occurs in some crops, so the disaster area cannot be directly extracted on DOY 273. In this study, images between DOY 161 and DOY 257 time are chosen. 113 typical disasters reported by insurance companies from 2011 to 2019 are selected as sample data. OTSU method is used to find the appropriate threshold value to extract disaster scope and verify its universal applicability through GEE monitoring model. We adopt the average value without the extreme outliers as the threshold to distinguish between disasters and non-disasters, and calculate the proportion between MODIS image extraction results and insured plots, so as to obtain the corresponding error size and verify its accuracy.

2.3.5 Disaster extraction

When the crops suffer from disasters, The values of $R_{NDVI\_TM(i)}$, $R_{NDVI\_AM(i)(j)}$ and $R_{NDVI\_ZM(i)(j)}$ will be slightly lower than the normal ones. Therefore, when the standardized value of a certain region

 doi:10.20944/preprints202007.0072.v1

model is less than a threshold value, the crop will be identified as affected by the disaster. The smaller the values of $R_{NDVI\_TM(i)}$, $R_{NDVI\_AM(i)(j)}$ and $R_{NDVI\_ZM(i)(j)}$ are, the more severe the damage will be. Thus, this study analyzed the data of $R_{NDVI\_TM(i)}$, $R_{NDVI\_AM(i)(j)}$ and $R_{NDVI\_AM(i)(j)}$ in Heilongjiang Province from 2010 to 2019 in accordance with the time sequence. The average value extracted by OTSU was taken as the threshold value, and the disaster scope was extracted from the corresponding disaster remote sensing monitoring model through the determined threshold values of each time phase. In view of the spatial resolution of MODIS data and the need to remove small patches after extraction of agricultural disasters, the disaster areas who covers less than 6 pixels (about 40 hectares) were eliminated to obtain the agricultural disaster scope of Heilongjiang Province from 2010 to 2019.

2.3.6 Accuracy verification

To test the accuracy of the scope of the disaster extracted by three kinds of disaster monitoring model, selecting DOY 285 fact-finding disasters during 2010-2019 as the validation sample, this study used the MODIS data date close to the moderate resolution of HJ-1a/1b CCD image NDVI value through the calculation of wave band operation and combines with the data reported by the insurance company, the changes of the NDVI value in the affected area and the affected area and the disaster scope extracted from the field data of agricultural disaster as the validation data. With a spatial resolution of 30m, the environment star image extracts the disaster scope whose precision is higher compared with the actual sampling results. Therefore, the disaster range extracted by this image is taken as the truth value to verify the accuracy of the extracted disaster range by MODIS image.

We take Absolute error =| Extract value - True value |, that is, the difference between the disaster result extracted from MODIS data and the disaster result extracted from environmental star image as the accuracy evaluation parameter. Finally, the errors of 285 verification samples in different models are calculated as the average values for accuracy test.

3. Results

3.1 phenological division of cultivated land

The purpose of taking the key phenological values as the basis for zoning is to combine the regions with similar phenological values as one region for study, and then conduct multi-scale segmentation within the cultivated land. After conducting many experiments and using segmentation evaluation index for calculation and analysis, we find that the ASEI value reaches the maximum when the optimal segmentation scale is 70. The finally obtained 39 phenological regions are shown in the following Figure 2. When the cultivated lands are categorized into regions according to their phenological values, the median values of different phenological regions are extracted from the processed images in GEE as $NDVIA_{MED(i)(j)}$, $NDVIZ_{MED(i)(j)}$, and then $R_{NDVI\_AM(i)(j)}$ and $R_{NDVI\_ZM(i)(j)}$ are calculated.

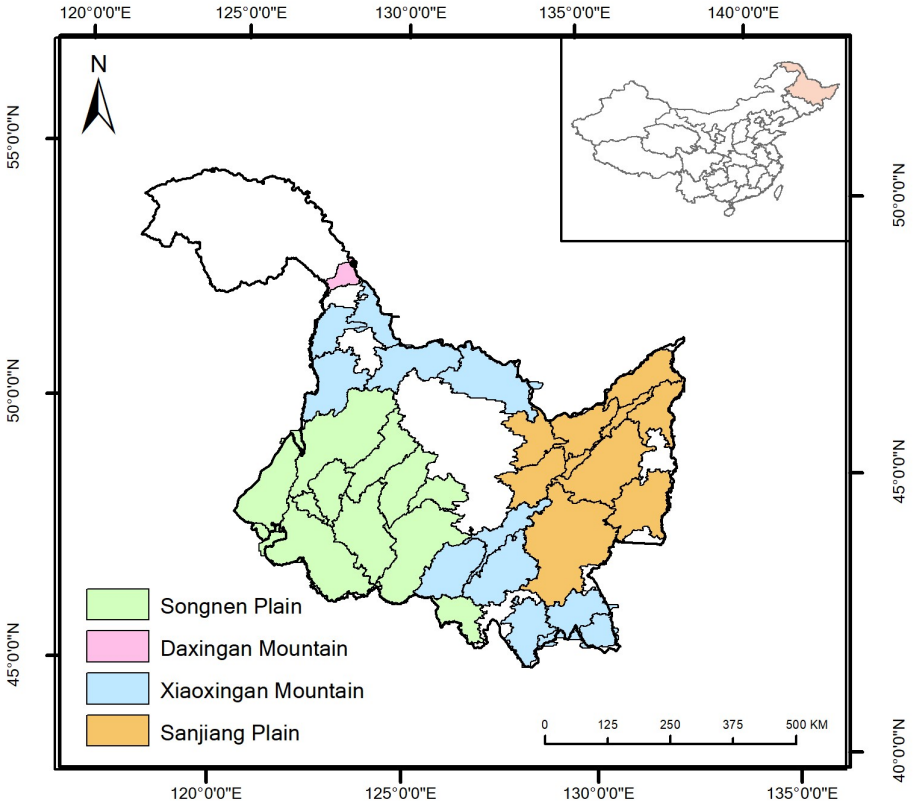

Figure 2. Phenological zoning in Heilongjiang Province

3.2 Precision analysis

How to determine the threshold value of disasters is a key issue for disaster scope extraction. We used OTSU method to extract the threshold value of DOY 113 sample points of different disaster types on GEE. From Table 3, we find that in the three models, the threshold size is mainly distributed between -0.1 ~-0.2. The thresholds extracted from different disaster types and by different models are different. The error in the table is received based on the difference between the proportion of disaster results extracted by environmental star image provided by the insurance company and the proportion of disaster results extracted by MODIS image. Among them, the errors of insect and wind disasters are larger. At the same time, we extracted the threshold value of insect and wind disasters after 16 days and conducted precision analysis. It was found that the errors of the results of these two disasters were smaller and the accuracy was higher through images observed after 16 days. Therefore, we used the images of 16 days later to calculate the threshold value of insect and wind disasters. The errors of hailstorm, drought disaster and flood disaster are small, so The MODIS image which is close to the time of disaster is used to calculate the disaster threshold for disaster monitoring.

 doi:10.20944/preprints202007.0072.v1

Table 3. Otsu extraction disaster threshold and disaster error analysis example

Model	Definition interpretation	Proportion of HJ-1A/b monitoring results in the insured land(%)	Threshold	Proportion of MODIS monitoring results in the insured land(%)	Error(%)
$R_{NDVI\_TM(i)}$	20170803Youyi hailstorm	1.31	-0.15	1.39	0.08
	20180703Tonghe flood	2.27	-0.16	2.36	0.09
	20160813Longjiang drought	0.47	-0.14	0.57	0.10
	20170802Fuyuan flood	0.17	-0.08	0.30	0.13
	20180703Zhaodong flood	13.14	-0.11	12.71	0.44
	20120702Maqiaohe hailstorm	84.82	-0.14	85.50	0.68
	20160702Hailstormun hailstorm	4.60	-0.15	3.88	0.73
	20160829Gannan drought	1.47	-0.16	0.66	0.82
	2018080Luobei wind hazard	2.47	-0.16	0.25	2.22
	20170901Beian wind hazard	16.63	-0.10	35.04	18.41
$R_{NDVI\_AM(i)(j)}$	20170803Youyi hailstorm	6.87	-0.10	10.96	4.09
	20180703Tonghe flood	2.27	-0.14	3.21	0.94
	20160813Longjiang drought	21.68	-0.14	25.74	4.06
	20170802Fuyuan flood	0.87	-0.17	0.77	0.10
	20180703Zhaodong flood	23.19	-0.14	19.32	3.88
	20120702Maqiaohe hailstorm	84.82	-0.17	89.06	4.24
	20160702Hailstormun hailstorm	54.57	-0.18	30.62	23.95
	20160829Gannan drought	1.47	-0.15	2.43	0.95
	2018080Luobei wind hazard	2.47	-0.15	0.63	1.84
$R_{NDVI\_ZM(i)(j)}$	20170803Youyi hailstorm	38.41	-0.13	51.15	12.73
	20180703Tonghe flood	6.87	-0.15	8.22	1.35
	20160813Longjiang drought	2.27	-0.14	1.79	0.48
	20170802Fuyuan flood	41.16	-0.14	63.13	21.98
	20180703Zhaodong flood	0.87	-0.13	0.97	0.10
	20120702Maqiaohe hailstorm	13.14	-0.11	17.28	4.14
	20160702Hailstormun hailstorm	84.82	-0.16	91.64	6.82
	20160829Gannan drought	36.25	-0.16	36.43	0.18
	2018080Luobei wind hazard	3.01	-0.16	3.74	0.73
	20170901Beian wind hazard	2.47	-0.18	0.47	1.99

 doi:10.20944/preprints202007.0072.v1

After removing the extreme values from the thresholds of different phases of the three monitoring models, the mean value was taken as the threshold value of the time phase. The size and error of average threshold are shown in Table 5. Generally speaking, as time goes by, the threshold value presents an increasing trend, which indicates that the disasters in the whole province show a trend of gradual reduction during the growing period of crops. In addition, the difference of the threshold value between $R_{NDVI\_AM(i)(j)}$ and $R_{NDVI\_ZM(i)(j)}$ at the same time phase is small, so the extraction disaster scopes may be similar. At the same time, as shown in Table 5. and Table 6. , according to whether environmental Star monitoring results or MODIS monitoring results, the proportion of hailstorm was the highest, followed by drought and flood disaster, while Wind disaster and insect disaster often account for a small part, namely, the disaster areas caused by them are small. On DOY 209, the relatively large average error may lead to a large error of disaster area extracted in this period. Having selected DOY 285 samples to test the accuracy of the three monitoring models, we calculated and found that the average precision of the $R_{NDVI\_TM(i)}$ monitoring model is 97.46%, the average precision of the $R_{NDVI\_AM(i)(j)}$ monitoring model is 96.90%, and the average precision of the $R_{NDVI\_ZM(i)(j)}$ monitoring model is 96.67%. In Table 6, the average errors of drought, wind disaster, hailstorm and flood disaster are smaller and the accuracy is higher, while the average error of insect infestation is larger and the accuracy is lower.

Table 4. Mean thresholds and error analysis of each phase

Model	DOY	Threshold	Average error (%)
$R_{NDVI\_TM(i)}$	177	-0.13	2.90
	193	-0.16	7.78
	209	-0.15	6.29
	225	-0.15	4.22
	241	-0.13	4.58
	257	-0.14	2.83
$R_{NDVI\_AM(i)(j)}$	177	-0.15	5.89
	193	-0.15	3.70
	209	-0.15	7.51
	225	-0.13	4.99
	241	-0.13	5.11
	257	-0.13	7.08
$R_{NDVI\_ZM(i)(j)}$	177	-0.16	5.27
	193	-0.16	4.32
	209	-0.15	7.44
	225	-0.13	5.31
	241	-0.15	3.16
	257	-0.13	4.06

 doi:10.20944/preprints202007.0072.v1

Table 5. Comparison sample table of the accuracy test of MODIS data disaster range extraction based on HJ-1A/B CCD image

Model	Definition interpretation	Proportion of HJ-1A/b monitoring results in the insured land(%)	Threshold	Proportion of MODIS monitoring results in the insured land(%)	Error (%)
$R_{NDVI\_TM(i)}$	20180801Tongjiang flood	7.08	-0.15	8.44	1.36
	20180803Tonghe wind hazard	3.41	-0.15	3.61	0.20
	20180803Suiling wind hazard	2.62	-0.15	1.79	0.83
	20160829Nehe drought	5.60	-0.13	0.86	4.73
	20120914Hulan Insect	20.36	-0.14	20.90	0.54
	20120829Wuchang Insect	8.79	-0.13	0.14	8.65
	2017090Nenjiang flood	12.35	-0.14	16.77	4.42
	20180901Zhaodong hailstorm	51.82	-0.14	58.66	6.84
	20180901Hailun hailstorm	52.13	-0.14	69.87	17.74
	20190907Nehe flood	22.34	-0.14	28.85	6.51
$R_{NDVI\_AM(i)(j)}$	20180801Tongjiang flood	4.10	-0.13	4.28	0.18
	20180803Tonghe wind hazard	8.55	-0.13	10.98	2.43
	20180803Suiling wind hazard	2.62	-0.13	3.22	0.60
	20160829Nehe drought	1.92	-0.13	1.06	0.86
	20120914Hulan Insect	20.36	-0.13	4.64	15.72
	20120829Wuchang Insect	8.79	-0.13	0.69	8.11
	20170901Nenjiang flood	6.94	-0.13	13.73	6.79
	20180901Zhaodong hailstorm	67.07	-0.13	70.06	2.98
	20180901Hailun hailstorm	80.72	-0.13	92.93	12.21
	20190907Nehe flood	50.25	-0.13	48.16	2.09
$R_{NDVI\_ZM(i)(j)}$	20180801Tongjiang flood	4.10	-0.13	4.73	0.63
	20180803Tonghe wind hazard	8.55	-0.13	10.98	2.43
	20180803Suiling wind hazard	2.62	-0.13	3.22	0.60
	20160829Nehe drought	1.92	-0.13	1.18	0.74
	20120914Hulan Insect	20.36	-0.13	1.80	18.55
	20120829Wuchang Insect	8.79	-0.13	12.41	3.62
	20170901Nenjiang flood	6.94	-0.13	8.53	1.58
	20180901Zhaodong hailstorm	67.07	-0.13	62.44	4.63
	20180901Hailun hailstorm	80.72	-0.13	91.63	10.90
	20190907Nehe flood	50.25	-0.13	42.80	7.45

 doi:10.20944/preprints202007.0072.v1

Table 6. Average errors of the three monitoring models for different disasters (%)

	$R_{NDVI\_TM(i)}$	$R_{NDVI\_AM(i)(j)}$	$R_{NDVI\_ZM(i)(j)}$
hailstorm	3. 16	2. 93	3. 52
pest plague	6. 70	11. 91	12. 33
wind hazard	1. 61	2. 28	1. 77
drought	4. 91	1. 68	5. 39
flood	2. 48	2. 85	2. 94

3.3 consistency analysis of applicability and extraction scope of different models

According to the thresholds of different time phases in Table 4, typical disasters verified by HJ-1A/B monitoring range and the disaster scope of Heilongjiang province from 2010 to 2019 were extracted. They are shown in Figure 4, Figure 5.

As shown in Table 6, , the average error of hailstorm and wind disasters extracted by $R_{NDVI\_TM(i)}$ and $R_{NDVI\_ZM(i)(j)}$ is relatively small, and in the actual observation in Figure 5, the disaster extraction range of $R_{NDVI\_TM(i)}$ and $R_{NDVI\_ZM(i)(j)}$ is similar. The average error of flood disasters extracted by $R_{NDVI\_AM(i)(j)}$ and $R_{NDVI\_ZM(i)(j)}$ is small, and in the actual observation the disaster extraction range of $R_{NDVI\_AM(i)(j)}$ and $R_{NDVI\_ZM(i)(j)}$ is similar. However, in terms of drought, although the error difference between $R_{NDVI\_TM(i)}$ and $R_{NDVI\_ZM(i)(j)}$ is smaller, the disaster range extracted by $R_{NDVI\_AM(i)(j)}$ is similar to that extracted by $R_{NDVI\_ZM(i)(j)}$ in actual observation.

The crops are ripe once a year in Heilongjiang Province, but the three models monitored and extracted the disaster areas from mid-June to mid-September with little difference. It can be seen from Table 7 that the three monitoring models have a similar ratio of phase disaster range to the cultivated land range of the whole province at time DOY 177-DOY 225, among which $R_{NDVI\_TM(i)}$ and $R_{NDVI\_ZM(i)(j)}$ have a small difference in the ratio of phase disaster range to the cultivated land range of the whole province on DOA 177, and Figure 4 shows that the disaster range extracted is also relatively close. In DOY 193-DOY 209 phases, there is a small difference between $R_{NDVI\_AM(i)(j)}$ and $R_{NDVI\_ZM(i)(j)}$ in the proportion of disaster scope in the cultivated land of the whole province, and the disaster scope extracted in Figure 4 was more consistent. In the phase of DOY 241-DOY 257, $R_{NDVI\_TM(i)}$ and the other two monitoring models shows that the extracted disaster range accounts for a larger percentage of the total cultivated land area in the province, and the extracted disaster range has a larger difference. The main reason is that at DOY 241-DOY 257, $R_{NDVI\_AM(i)(j)}$ and $R_{NDVI\_ZM(i)(j)}$ are more sensitive to waterlogging so the monitored range is larger.

Table 7. Ratio of disaster scope to cultivated land area in Heilongjiang Province in 2017(%)

	$R_{NDVI\_TM(i)}$	$R_{NDVI\_AM(i)(j)}$	$R_{NDVI\_ZM(i)(j)}$
177	11. 29	14. 17	11. 83
193	8. 04	7. 22	6. 78
209	6. 03	4. 41	4. 06
225	3. 17	4. 38	3. 97
241	5. 96	10. 30	11. 58
257	11. 43	18. 59	16. 85

3.4 Analysis of spatial and temporal pattern of disasters in the study area

 doi:10.20944/preprints202007.0072.v1

3.4.1 Spatial and temporal pattern analysis of disasters in 2017 in the research area

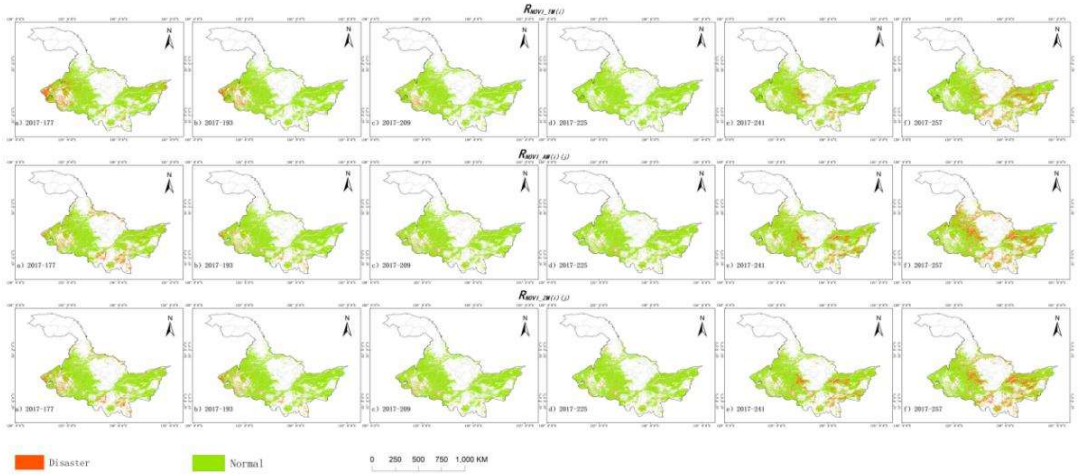

Figure 4. Disaster distribution map of the province in 2017 for the three monitoring models

After extracting the disaster area of Heilongjiang province with the threshold value of different time phase, the temporal and spatial distribution of disasters in Heilongjiang province in the past ten years can be analyzed. Take 2017 as an example, as shown in Figure 4, disasters in June were concentrated in the western and southeastern regions. Longjiang county and Tailai county had little rain over the years, and drought occurred frequently. In early July, the situation of crops turned better, but the disaster was still serious in southern areas such as Wuchang and other places due to the heavy rain, as well as in Keshan county, Nehe city and some areas. In late July crops grew well, and the disasters were concentrated in the western and northwestern areas of Heilongjiang Province, while the southeastern area of Fuyu County had low vegetation index in the whole July, and disasters occurred. In mid-August, the vegetation growth in Jiamusi and Suihua areas was poor, and the trend worsen in early September

From the perspective of the spatial and temporal distribution trend of disasters, according to the consistency of the distribution, the time period DOY 177-DOY 193 was called time period 1, the time period DOY 193-DOY 209 period 2, the time period DOY 209-DOY 225 period 3, and the time period DOY 225-DOY 257 period 4. From the time variation characteristics of provincial disasters, the disaster area showed a downward trend from period 1 to period 2, and this trend continues to period 3 and hits the lowest point. On the contrary, entering period 4, the disaster area increased rapidly, which was consistent with the change of the disaster area of the insured land in the whole province. In period 1 the disaster was mainly distributed in the west and south, among which Qiqihar, Heihe, Daqing, Mudanjiang, Anda and Wudalianchi were severely affected, and the level of severity gradually decreases. In the second period, agricultural disasters were mainly concentrated in Qiqihar, Heihe (Aihui District, Nenjiang County, Xunke County, Sunwu County, Wudalianchi City), Suihua ,Nehe and other places, which were severely influenced. In the third period, the disasters mainly showed in the west, south and central part of Heilongjiang Province. Qiqihar and Heihe were still the main affected areas, jixi, Jiamusi and Suihua were stricken obviously, and Duerbert, Zhaozhou and Acheng were severely suffered. During the period 4, because in late August early September, crops in many areas had already entered the harvest season, especially the rice crops which is grown widely in Sanjiang region in Jiamusi built , leading to a significant increase of disaster area in Kiamusze region from Figure 4. It caused the impression that agricultural disasters in Heilongjiang province focus in the northeast in Figure 4. To sum up, agricultural disasters in Heilongjiang province in 2017 mainly concentrated in the northeast, south, west and central regions.

Preprints (www.preprints.org) | NOT PEER-REVIEWED | Posted: 5 July 2020 doi:10.20944/preprints202007.0072.v1

3.4.2 Spatial and temporal disaster pattern analysis of different phases in the study area from 2010 to 2019

(a)

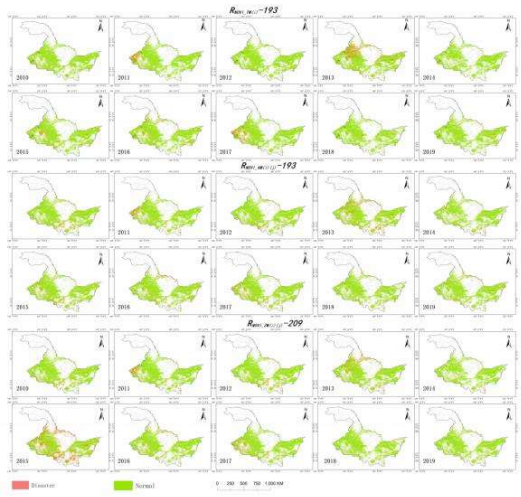

(b)

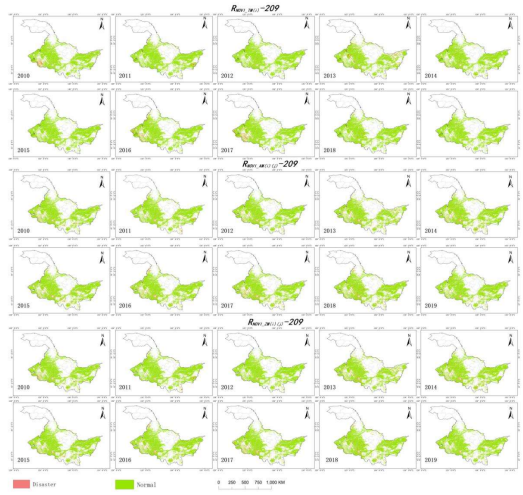

(c)

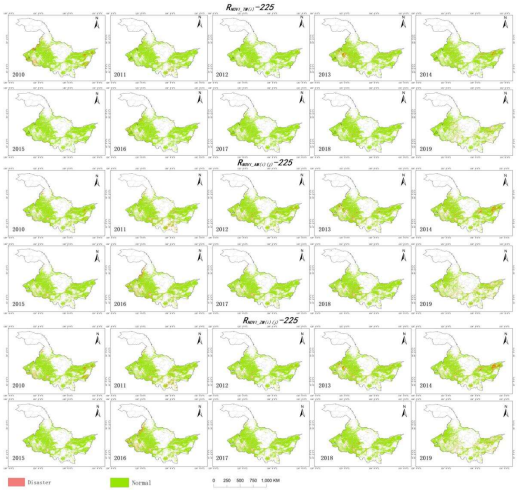

(d)

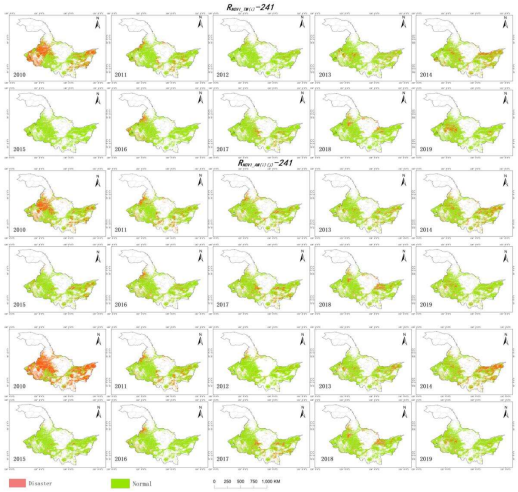

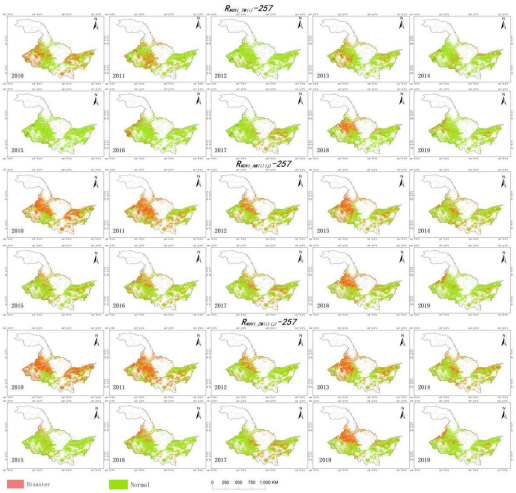

 doi:10.20944/preprints202007.0072.v1

(e) **(f)**

Figure 5. Disaster distribution map of the province with different phases from 2010 to 2019 (a: DOY 177, b: DOY 193, c: DOY 209, d: DOY 255, e: DOY 241, f: DOY 257)

Through the comparison of the same time phase images in different years, we can have a more profound analysis of the spatial and temporal pattern distribution of disasters.

Through the analysis of disasters in the ten years, we can see that on DOY 177 in 2010, 2011, 2012, 2016 and 2017 have a large range of disasters. In 2010, the spring and winter of Heilongjiang Province continued to have low temperature. The weather warmed late and the soil defrosted slowly. In May, precipitation was unusually high, leading to late field seeding. Therefore, the bare soil area was large, causing the large disaster scope obtained in 2010 shown in Figure 5 (a). The severe convective weather caused the hailstorm in Beilin district of Suihua city, Hailun city, Lanxi county, Qingan county, Suiangxian county and Hulan district of Harbin city. The actual range of hailstorm is consistent with that extracted of the three models. Because of the sustained high temperature and less rain from late May to June, parts of Songnen plain, north forest region, north of Sanjiang plain, and Mudanjiang were in the drought. The drought-stricken areas were mainly distributed in the Greater Hinggan Mountains and Mudan River. In Mudan River region three monitoring model have the consistency. However, $R_{NDVI\_AM(i)(j)}$ and $R_{NDVI\_ZM(i)(j)}$ for forest region is more sensitive to drought monitoring, so extraction to the drought in northern scope is bigger. In June 2011, rainstorm and flood disaster occurred in Heilongjiang Province, and Fujin, Qiqihar and other areas were affected seriously. Besides, hailstorm occurred in many places. It is shown in Figure 5 (a) that the disaster area extracted in 2011 is concentrated in the west and northeast of Heilongjiang Province, which is consistent with meteorological data. In June 2012, the precipitation in the eastern part of Harbin and the Sanjiang Plain continued to be low, finally resulting in drought. Shuangyashan, Baoqing, Wuchang, Tonghe, Fangzheng and other counties suffered from severe drought. Hailstorm broke out in Qiqihar Mountain County. In Figure 5 (a), the disaster areas extracted in 2012 area concentrated in the eastern and western parts of Heilongjiang Province, and the extraction of drought areas turns out to be good. In June 2014, strong convective weather occurred in some areas in Heilongjiang Province. Wind disaster and hailstorms occurred with high frequency, wide impact range and severe losses. Through The extraction it can be found that the disasters concentrated in Jiamusi area which is in the south of the province and Suihua city which is in the western part. In June 2015, strong convective weather occurred in Heilongjiang Province with high frequency of hailstorm. The extracted disasters are concentrated in the northwest, northeast and south of Heilongjiang Province. In June 2016, there was a lot of precipitation in Heilongjiang province, with heavy rain concentrated in most of Songnen plain and the north of Sanjiang plain. Yanshou county and other places suffered from the severe waterlogging because of the rain, and the meteorological disaster was consistent with the extraction disaster in this county. In mid-June 2017, rainstorms and floods occurred frequently, and waterlogging was severe in Nehe city and other places, which was consistent with the monitoring results.

During the time phase DOY 193- DOY 209, disasters happened in 2012, 2015, 2016 and 2017 were relatively serious. In 2010, the average rainfall of Heilongjiang province was higher than that of the whole year. The rainstorms and floods in July damaged 221,000 hectares of crops. It is shown in Figure 5 (b) that in 2010 floods were mainly occurred in Heihe, Suihua and Harbin. From May to mid-July 2012, rainfall in the eastern part of Harbin and the Sanjiang plain continued to be low, causing moderate meteorological drought, including severe drought in Shuangyashan urban area and Baoqing, Fuchang, Tonghe, Fangzheng and other counties. At the end of July, Daqing and many other cities suffered from severe flood and waterlogging disaster, which is consistent with the disaster extraction range. In addition, there were mild disasters in the central and northern regions of the extraction range. In July 2013, heavy rainfall occurred in Heilongjiang Province, causing regional floods in Heilongjiang, Nenjiang and Songhua rivers. In the disaster distribution map, it is obvious that greater waterlogging showed along the river. Strong convective weather had been seen in some

areas in Heilongjiang province. In the end of July, hailstones hit Beilin district of Suihua city, which is consistent with the disaster area extracted. In July 2014, Jiamusi was hit by severe hailstorms, also consistent with the extracted disaster scope. Meanwhile, according to the extracted disaster map, it could be found that the whole province was flooded and the waterlogging was serious during this period. In 2015, Heilongjiang Province had witnessed frequent rainstorms and floods, and severe convective weather occurred in many areas. For example, Harbin Hulan district was hit by tornadoes and hail. In mid-July, Hulin city was hit by a rainstorm, conforming to the the disaster area extracted on DOY 209. In addition, there are a few disasters in the northeast of Heilongjiang Province. In July 2016, the continuous high temperature and low rainfall in Heilongjiang province led to a drought in the west of the Songnen plain in mid-July. Rainstorms and floods occurred frequently, especially in late July, mainly in most parts of Songnen plain and the north of Sanjiang plain. These are all consistent with the extraction disaster scope. Besides, there is a small disaster in the northwest on DOY 209. In July 2017, the average temperature was too high, so most of the Songnen plain was arid. In the middle of the year, the western region suffered from a continuous drought due to insufficient precipitation. At the end of July, so did Duerbert, Zhaozhou, Zhaoyuan and Acheng. Heavy rain and floods arised frequently in the middle and late July. In addition to tornadoes in Suihua, short-term heavy rain, strong winds and hail attacked In Aihui district of Heihe city, Nenjiang county, Xunke county, Sunwu county and Wulianchi city. It can be seen from the disaster distribution map that the disaster in western China is more serious while the disaster in Heihe is relatively light.

During the time phase DOY 225-DOY 241, disasters appeared in 2011, 2015, 2016 and 2017, were relatively serious. In August 2010, heavy rains and floods happened frequently in Qiqihar and Hegang. In the provincial distribution map extracted on DOY 225, in addition to the above disasters consistent with meteorological data, a large range of disasters exist in the east and northeast of Heilongjiang Province. At the end of August 2011, a severe meteorological drought occurred in the eastern region, mainly in Mudanjiang, Harbin, Shuangyashan, Hulin and other places, and especially in Linkou and Muling. It is consistent with the disaster range extracted in 2011 in Figure 5(e). Meanwhile, it can be seen from the figure that Heihe river in the northwest also experienced a serious disaster. At the end of August 2012, a wind disaster caused large areas of crop lodging in cities and counties in the central part of Suihua and Sanjiang Plain, resulting in serious urban waterlogging in Harbin. From the extracted disaster map, it can be seen that, except for the disasters consistent with the above meteorological data, the flood in Sanjiang Plain is relatively serious. In the summer of 2013, Heilongjiang Province possessed a high level of precipitation. In the middle of August, Fuyuan county was stricken by flood and waterlogging and suffered serious losses, which is in agreement with the distribution map of extracted disaster in the whole province. Beyond that, the eastern part of Heilongjiang province has suffered from a large range of disasters. At the end of August 2016, strong winds and rainstorms hit the eastern part of Heilongjiang province. Gusts in Tongjiang even reached level 10, Fuyuan, Suibin, Fujin and Huachuan Gusts level 9, Tonghe, Dongning and other 13 counties and cities level 8, and Suifenhe, Yilan and other 30 counties and cities level 7. The high winds caused partial lodging of rice and corn crops. The above-mentioned information is consistent with the extraction range. In August 2017, the amount of precipitation in Heilongjiang Province has increased. In mid-August, a severe flood was seen in The city of Anda, and it also occurred in a number of small and medium-sized rivers, including The Tongkan, Hulan, Zhaolanxin, Belahong, Maolan, Dongxiao and Helen rivers, with their water levels rising rapidly. In the disaster distribution map of the whole province on DOY 247, the flood was serious.

On DOY 257, The disasters in 2010 and 2019 were still serious. In 2010, droughts occurred in Heilongjiang Province from late spring to early summer and September. As shown in Figure 5 f), the 2010 disaster map shows that disasters are mainly presented in Sanjiang plain and the eastern part of Heilongjiang Province. Since the fall of 2011, the continuous high temperature and little rain in Heilongjiang Province led to meteorological drought in some areas. The disaster monitoring results extracted in 2011 are primarily shown in the east. In the middle of September 2012, Typhoon "Sanba" moved northward and disturbed the normal situation in the eastern part of Heilongjiang Province. The precipitation alleviated the previous drought and water shortage of reservoirs in the eastern part

Preprints (www.preprints.org) | NOT PEER-REVIEWED | Posted: 5 July 2020 doi:10.20944/preprints202007.0072.v1

of Heilongjiang Province. Furthermore, the level precipitation in September was high. From the disaster scope extraction map waterlogging can be seen being caused by serious river flooding. However, because rice was harvested early in some areas, the disaster range of phase extraction may be large. [33]

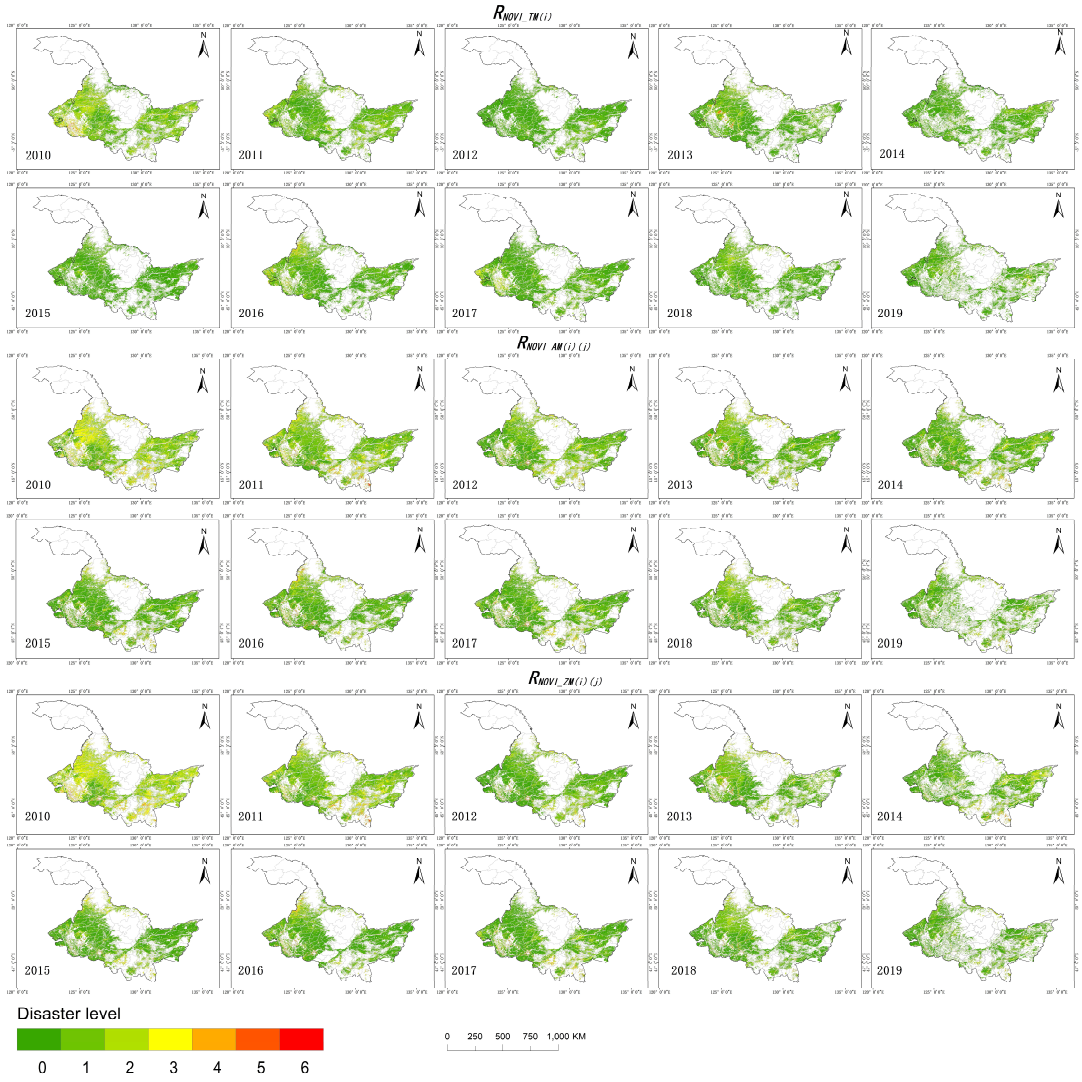

Figure 6. Disaster classification in Heilongjiang Province

It can be seen from Figure 5, Figure 6 and meteorological data analysis that according to the distribution of disasters throughout the year, 2010, 2011 and 2012 are normal preference years .In 2014, 2015, 2017 and 2018, disasters were relatively mild. Disasters in 2013, 2016 and 2019 were serious.

By analyzing the meteorological disaster data, Figure 5 and Figure 6 as well as the above discussion, we summarized the spatial and temporal distribution characteristics of disasters from 2010 to 2019 in Heilongjiang Province: in terms of time distribution, disasters occurred frequently in July and August; from the perspective of spatial distribution, disasters were mainly occurred in the central and eastern regions and the southwest regions from June to August, including Qiqihar, Heihe, Suihua, Haerbin, Jiamusi and other places.

Different disasters have different spatial and temporal distribution characteristics: The submersion is seen frequently in late June, but it also occurs in July and August, except for the Northwest Greater Khingan Mountains. In some years, submersion is strong in September. This kind of disaster Mainly distributed in the northeast of Heilongjiang, such as Jiamusi, Tongjiang, Fuyuan,

Fujin and Suiang county of Hegang. In addition, Shuangyashan, Qiqihar in the west, Daqing and Suihua in the southwest are also frequently flooded. This is due to the fact that precipitation in Black Dragon Province is concentrated from June to August, and the terrain that it is high in the northwest, north and southeast, and low in the northeast and southwest. That means, according to the precipitation, a big difference exists between the eastern and western regions in Heilongjiang province all year round, with a high level of precipitation in the eastern and western regions and low in the central and southern regions. Songnen plain and Sanjiang plain have a higher topographical terrain and favorable water vapor conditions, easy to form large precipitation, butthere are also many flood disasters. At the same time, since the central and northwest areas are high while the northeast and west are low in the province, flood is easy to occur.

Hail disasters occur frequently in June and July, and from late August to mid-September. Jiamusi in the east is a frequent disaster site, so are Shuangyashan, Mudanjian and, Jixi. In the West hail disasters concentrated in Suihua, Heihe, Qiqihar area. The mountain area represented by the Greater Hinggan Mountains has low temperature and is prone to suffer from frost and hail disasters. It is mainly formed due to the air lift caused by topography and the planting structure of crops.

The drought in Heilongjiang province mainly occurred in July and September, with the July drought mainly showed in the southwest Suihua urban area, Harbin and Daqing Durbert Mongolian Autonomous County, Zhaozhou County and Zhaoyuan County. In the northwest, Baoqing County, Suibin County, Fujin City, Tongjiang City and Fuyuan County are located in the Sanjiang Plain area. In September, it was mainly occured in the northeast, including Yichun city and Hegang City in the north, Lubei County, Suibin County and Tongjiang City. Qiqihar and Mudanjiang area have a high temperature and are prone to drought.

Wind damages are always seen in August and September while fewer in July in Heilongjiang Province. This type of disasters mainly happened in the east and northeast, as well as central and eastern regions such as Huachuan county, Suijiang county, Fujin city, Tongjiang city and Fuyuan county in Jiamusi,, Yilan county, Shuangyashan jixian county, Baoqing, RaoHe city, Jidong county, the basic data of Jixi and Hulin.

4. Discussion

In general, the three disaster monitoring models have high accuracy, but their monitoring accuracy for various disasters is different. The monitoring accuracy of hailstorm, drought and flood disaster is higher. For insect and wind disasters, the real-time monitoring accuracy is low, and the phenomenon of disaster lag usually appears in the next scene image after 16 days. This is because the disasters caused by hailstorm, flood disaster and drought for crops are immediate and serious, with short duration and obvious changes in the image. However, the damage caused by insect pests and wind disasters to crops is not short-term but continuous, and it is not able to change immediately in the image.

The accuracy of disaster extraction range of different phases is also different. According to the extraction difference of disaster range in table 7, the disaster range on DOY 130, DOY 145, DOY 167,and DOY 273 present great differences and the range itself is large, and the consistence merely shows from DOY 177 to DOY 257. This is mainly due to the low crop coverage and large bare soil area before mid June; Meanwhile, in September when the rice and other crops entered the tasseling stage, and some crops were premature, it led to the phenomenon of "no yield" on the image after the large area of rice was harvested. Therefore, the vegetation index of the three monitoring models in this area was relatively low. In late August, rice was harvested in advance in some areas of Heilongjiang Province, but the range was small, leading to a large disaster scope extracted on DOY 241 in some small areas. On DOY 247, this range is further expanded, bringing a further increase in disaster extraction range error. Among the three models, $R_{NDVI\_AM(i)(j)}$ is highly sensitive to bare soil, and the disaster range that can be easily extracted on DOA 177 and DOA 257 is relatively large.

Looking at the applicability and consistency of the three monitoring models for different disasters, we can find that $R_{NDVI\_TM(i)}$ and $R_{NDVI\_ZM(i)(j)}$ have a higher monitoring precision and a similar

extraction rang for hailstorm and wind disaster, and $R_{NDVI\_AM(i)(j)}$ and $R_{NDVI\_ZM(i)(j)}$ for flood and drought. It is vulnerable to flooding in August and September, which results in a greater range of disasters than $R_{NDVI\_TM(i)}$ extraction. This may be due to the mechanism of different monitoring models. $R_{NDVI\_AM(i)(j)}$ is more about comparing the current crop growth with the historical average. In this model, the standard value is determined based on the median NDVI value of multi-year vegetation. The main defect is that the life span is long so the planting structure of crops may change, which will affect the standard value. $R_{NDVI\_AM(i)(j)}$ pays more attention to describing the average growth of crops compared to different phenological areas. Compared with $R_{NDVI\_TM(i)}$, $R_{NDVI\_AM(i)(j)}$ doesn't take the historical growth of the crop into consideration. $R_{NDVI\_ZM(i)(j)}$, which combines the characteristics of the above two methods, reflects not only the level growth of crops compared with the historical average level, but also the average growth in this phenological area. Therefore, $R_{NDVI\_TM(i)}$ and $R_{NDVI\_ZM(i)(j)}$ have good consistency in hailstorm disaster and wind disaster, while $R_{NDVI\_AM(i)(j)}$ and $R_{NDVI\_ZM(i)(j)}$ in flood disaster.

There are some common problems in the extraction of disaster scope extracted by the three monitoring models, namely, the low, spatial resolution results in the existence of mixed pixels and then the low detection accuracy of some small-scale agricultural disasters. higher spatial resolution and temporal resolution monitoring methods can be adopted to improve the monitoring accuracy. At the same time, the planting structure and growth period differences of different crop types were not fully considered in the study

In the future research, the data of planting structure of the whole province can be combined for further detailed analysis. In addition, the study should continue to take advantage of rapidness, a wide range and good portability of GEE, and expand the study area to try to conduct disaster monitoring analysis on the global farmland scope or compare the differences of disasters in the same latitude area and analyze the law and reason. Higher resolution images can also be used to model NDVI, as well as higher resolution validation data. It provides technical support for disaster early warning, disaster prevention and mitigation as well as post-disaster rescue work through the extraction of such large scale and long time series of disaster scope.

5.Conclusions

In this study, the $R_{NDVI\_TM(i)}$ model, $R_{NDVI\_AM(i)(j)}$ model and $R_{NDVI\_ZM(i)(j)}$ model were built through Google Earth Engine platform to extract the disaster scope from 2010 to 2019 in Heilongjiang Province. Meanwhile, the temporal and spatial pattern changes and applicability of different models to disasters were studied in combination with meteorological data. The results show that:

1. $R_{NDVI\_TM(i)}$ model, $R_{NDVI\_AM(i)(j)}$ model and $R_{NDVI\_ZM(i)(j)}$ model can extract the spatial-temporal features of large-scale disasters with high precision, which is consistent with the disaster situation and time variation trend reported by the whole province, and achieves the ideal result of disaster range extraction based on MODIS data.

2. $R_{NDVI\_TM(i)}$ model, $R_{NDVI\_AM(i)(j)}$ model and $R_{NDVI\_ZM(i)(j)}$ model have different applicability to hailstorm, floods, drought, insect disaster and wind disaster, and different extraction range of disaster. In addition, there is a strong consistency between DOY 177 and DOY 257, and the extraction disaster range is close.

3. The disaster scope extracted by $R_{NDVI\_TM(i)}$ model, $R_{NDVI\_AM(i)(j)}$ model and $R_{NDVI\_ZM(i)(j)}$ is in good agreement with the meteorological disaster data of Heilongjiang Province, which can be used to analyze the space-time pattern of disasters and provide support for disaster risk partition.

Author Contributions: Zhengrong Liu and Huanjun Liu; Investigation, Zhengrong Liu; Methodology, Zhengrong Liu; Resources, Chong Luo and Yongchol Ju; Visualization, Zhengrong Liu and Haoxuan Yang; Writing – original draft, Zhengrong Liu; Writing – review & editing, Huanjun Liu and dong Guo.

Funding: This research was funded by Special Foundation for Basic Research Program in wild China of CAS, grant number XDA23070501.

Conflicts of Interest: The authors declare no conflict of interest.

References

References must be numbered in order of appearance in the text (including citations in tables and legends) and listed individually at the end of the manuscript. We recommend preparing the references with a bibliography software package, such as EndNote, ReferenceManager or Zotero to avoid typing mistakes and duplicated references. Include the digital object identifier (DOI) for all references where available.

Citations and References in Supplementary files are permitted provided that they also appear in the reference list here.

In the text, reference numbers should be placed in square brackets [ ], and placed before the punctuation; for example [1], [1–3] or [1,3]. For embedded citations in the text with pagination, use both parentheses and brackets to indicate the reference number and page numbers; for example [5] (p. 10), or [6] (pp. 101–105).

1. Campbell B M, Vermeulen S J, Aggarwal P K, et al. Reducing risks to food security from climate change[J]. Global Food Security, 2016, 11: 34-43
2. Meng J, Du X, Wu B. Generation of high spatial and temporal resolution NDVI and its application in crop biomass estimation[J]. International Journal of Digital Earth, 2013, 6(3): 20418.
3. Garonna I, de Jong R, Schaepman M E. Variability and evolution of global land surface phenology over the past three decades (1982–2012)[J]. Global Change Biology, 2016, 22(4): 1456-1468
4. Qu C, Hao X, Qu J J. Monitoring extreme agricultural drought over the Horn of Africa (HOA) using remote sensing measurements[J]. Remote Sensing, 2019, 11(8): 902.
5. Hazaymeh K, Hassan Q K. A remote sensing-based agricultural drought indicator and its implementation over a semi-arid region, Jordan[J]. Journal of Arid Land, 2017, 9(3): 319-330.
6. Ahmed M R, Hassan Q K, Abdollahi M, et al. Introducing a New Remote Sensing-Based Model for Forecasting Forest Fire Danger Conditions at a Four-Day Scale[J]. Remote Sensing, 2019, 11(18): 2101.
7. Chowdhury, E., & Hassan, Q. (2015). Development of a new daily-scale forest fire danger forecasting system using remote sensing data. *Remote Sensing*, *7*(3), 2431-2448.
8. Fox D M, Carrega P, Ren Y, et al. How wildfire risk is related to urban planning and Fire Weather Index in SE France (1990–2013)[J]. Science of the total environment, 2018, 621: 120-129.
9. Di S, Guo L, Lin L. Rapid Estimation of Flood Crop Loss by Using DVDI[C]//2018 7th International Conference on Agro-geoinformatics (Agro-geoinformatics). IEEE, 2018: 1-4.
10. Olsson P O, Lindström J, Eklundh L. Near real-time monitoring of insect induced defoliation in subalpine birch forests with MODIS derived NDVI[J]. Remote Sensing of Environment, 2016, 181: 42-53.
11. Dutta D, Kundu A, Patel N R, et al. Assessment of agricultural drought in Rajasthan (India) using remote sensing derived Vegetation Condition Index (VCI) and Standardized Precipitation Index (SPI)[J]. The Egyptian Journal of Remote Sensing and Space Science, 2015, 18(1): 53-63.
12. Bayarjargal Y, Karnieli A, Bayasgalan M, et al. A comparative study of NOAA–AVHRR derived drought indices using change vector analysis[J]. Remote Sensing of Environment, 2006, 105(1): 9-22.
13. Quiring S M, Ganesh S. Evaluating the utility of the Vegetation Condition Index (VCI) for monitoring meteorological drought in Texas[J]. Agricultural and Forest Meteorology, 2010, 150(3): 330-339.
14. Kogan F N. Application of vegetation index and brightness temperature for drought detection[J]. Advances in space research, 1995, 15(11): 91-100.
15. Sholihah R I, Trisasongko B H, Shiddiq D, et al. Identification of agricultural drought extent based on vegetation health indices of Landsat data: case of Subang and Karawang, Indonesia[J]. Procedia Environmental Sciences, 2016, 33: 14-20.
16. Karnieli A, Agam N, Pinker R T, et al. Use of NDVI and land surface temperature for drought assessment: Merits and limitations[J]. Journal of climate, 2010, 23(3): 618-633.

17. Sandholt I, Rasmussen K, Andersen J. A simple interpretation of the surface temperature/vegetation index space for assessment of surface moisture status[J]. Remote Sensing of environment, 2002, 79(2-3): 21424
18. Patel N R, Anapashsha R, Kumar S, et al. Assessing potential of MODIS derived temperature/vegetation condition index (TVDI) to infer soil moisture status[J]. International Journal of Remote Sensing, 2009, 30(1): 23-39.
19. Gao Z, Gao W, Chang N B. Integrating temperature vegetation dryness index (TVDI) and regional water stress index (RWSI) for drought assessment with the aid of LANDSAT TM/ETM+ images[J]. International Journal of Applied Earth Observation and Geoinformation, 2011, 13(3): 495-503.
20. García-Tejero I F, Hernández A, Padilla-Díaz C M, et al. Assessing plant water status in a hedgerow olive orchard from thermography at plant level[J]. Agricultural Water Management, 2017, 188: 50-60.
21. Dahlgren R P, Vanderbilt V C, Daughtry C S T. Estimates of Leaf Relative Water Content from Optical Polarization Measurements[J]. AGUFM, 2017, 2017: A21B-2160.
22. Zhao S, Cong D, He K, et al. Spatial-temporal variation of drought in China from 1982 to 2010 based on a modified temperature vegetation drought index (mTVDI)[J]. Scientific Reports, 2017, 7(1): 1-12.
23. Liu S, Tian J, Wang S, et al. Crop Drought Area Extraction Based On Remote Sensing Time Series Spatial-Temporal Fusion Vegetation Index[C]//IGARSS 2019-2019 IEEE International Geoscience and Remote Sensing Symposium. IEEE, 2019: 6271-6274.
24. Feng M, Guo X, Wang C, et al. Monitoring and evaluation in freeze stress of winter wheat (Triticum aestivum L.) through canopy hyperspectrum reflectance and multiple statistical analysis[J]. Ecological indicators, 2018, 84: 290-297.
25. Wang H, Huo Z, Zhou G, et al. Estimating leaf SPAD values of freeze-damaged winter wheat using continuous wavelet analysis[J]. Plant physiology and biochemistry, 2016, 98: 39-45.
26. Zheng X, Song P, Li Y, et al. Monitoring Locusta migratoria manilensis damage using ground level hyperspectral data[C]//2019 8th International Conference on Agro-Geoinformatics (Agro-Geoinformatics). IEEE, 2019: 1-5
27. Rahman M S, Di L. A Systematic Review on Case Studies of Remote-Sensing-Based Flood Crop Loss Assessment[J]. Agriculture, 2020, 10(4): 131.
28. Di L, Yu E, Shrestha R, et al. DVDI: A new remotely sensed index for measuring vegetation damage caused by natural disasters[C]//IGARSS 2018-2018 IEEE International Geoscience and Remote Sensing Symposium. IEEE, 2018: 9067-9069.
29. Klisch A, Atzberger C. Operational drought monitoring in Kenya using MODIS NDVI time series[J]. Remote Sensing, 2016, 8(4): 267.
30. Winkler K, Gessner U, Hochschild V. Identifying droughts affecting agriculture in Africa based on remote sensing time series between 2000–2016: rainfall anomalies and vegetation condition in the context of ENSO[J]. Remote Sensing, 2017, 9(8): 831.
31. Nagy A, Fehér J, Tamás J. Wheat and maize yield forecasting for the Tisza river catchment using MODIS NDVI time series and reported crop statistics[J]. Computers and Electronics in Agriculture, 2018, 151: 41-49.
32. Pekel J F, Ceccato P, Vancutsem C, et al. Development and application of multi-temporal colorimetric transformation to monitor vegetation in the desert locust habitat[J]. IEEE Journal of selected topics in applied earth observations and remote sensing, 2010, 4(2): 318-326.
33. Zhao J L, Zhang D Y, Luo J H, et al. Detection and mapping of hail damage to corn using domestic remotely sensed data in China[J]. Australian Journal of Crop Science, 2012, 6(1): 101.
34. Zhou J, Pavek M J, Shelton S C, et al. Aerial multispectral imaging for crop hail damage assessment in potato[J]. Computers and Electronics in Agriculture, 2016, 127: 406-412.
35. Chen H, Liang Q, Liang Z, et al. Remote-sensing disturbance detection index to identify spatio-temporal varying flood impact on crop production[J]. Agricultural and Forest Meteorology, 2019, 269: 180-191.
36. Löw F, Waldner F, Latchininsky A, et al. Timely monitoring of Asian Migratory locust habitats in the Amudarya delta, Uzbekistan using time series of satellite remote sensing vegetation index[J]. Journal of environmental management, 2016, 183: 562-575.

37. Allevato E, Saulino L, Cesarano G, et al. Canopy damage by spring frost in European beech along the Apennines: effect of latitude, altitude and aspect[J]. Remote Sensing of Environment, 2019, 225: 431-440.
38. Huang Q, Wu W, Zhang L, et al. MODIS-NDVI-based crop growth monitoring in China agriculture remote sensing monitoring system[C]//2010 Second IITA International Conference on Geoscience and Remote Sensing. IEEE, 2010, 2: 287-290.
39. Li C, Li H, Li J, et al. Using NDVI percentiles to monitor real-time crop growth[J]. Computers and Electronics in Agriculture, 2019, 162: 357-363.
40. Chakraborty S, Weindorf D C, Deb S, et al. Rapid assessment of regional soil arsenic pollution risk via diffuse reflectance spectroscopy[J]. Geoderma, 2017, 289: 72-81
41. Sun W, Zhang X. Estimating soil zinc concentrations using reflectance spectroscopy[J]. International journal of applied earth observation and geoinformation, 2017, 58: 126-133.
42. Mutanga O, Kumar L. Google Earth Engine Applications[J]. Remote Sensing, 2019, 11(5).
43. Beaton A, Whaley R, Corston K, et al. Identifying historic river ice breakup timing using MODIS and Google Earth Engine in support of operational flood monitoring in Northern Ontario[J]. Remote sensing of environment, 2019, 224: 352-364.
44. Kumar L, Mutanga O. Google Earth Engine applications since inception: Usage, trends, and potential[J]. Remote Sensing, 2018, 10(10): 1509.
45. Sazib N, Mladenova I, Bolten J. Leveraging the google earth engine for drought assessment using global soil moisture data[J]. Remote Sensing, 2018, 10(8): 1265.
46. Liu C C, Shieh M C, Ke M S, et al. Flood prevention and emergency response system powered by google earth engine[J]. Remote sensing, 2018, 10(8): 1283.
47. Pradhan B, Moneir A A A, Jena R. Sand dune risk assessment in Sabha region, Libya using Landsat 8, MODIS, and Google Earth Engine images[J]. Geomatics, Natural Hazards and Risk, 2018, 9(1): 1280-1305.
48. Lu L, Wu C, Di L. Exploring the Spatial Characteristics of Typhoon-Induced Vegetation Damages in the Southeast Coastal Area of China from 2000 to 2018[J]. Remote Sensing, 2020, 12(10): 1692.
49. Fu Q, Zhou Z, Li T, et al. Spatiotemporal characteristics of droughts and floods in northeastern China and their impacts on agriculture[J]. Stochastic Environmental Research and Risk Assessment, 2018, 32(10): 2914931.
50. Zhenxiang X, Zhaorui Y, Qiang F, et al. Characteristics and risk assessment of agricultural meteorological disasters based on 30 years' disaster data from Heilongjiang Province of China[J]. International Journal of Agricultural and Biological Engineering, 2017, 10(6): 144-154.
51. Liu Huanjun, Yan Yan, Zhang Xinle, Qiu Zhengchao, Wang Nan, & Yu Wei. (2017). Remote Sensing Extraction of Crop Planting Structure for Agricultural Regionalization. China Agricultural Resources and Regional Planning, 38 (8), 43-564.
52. China Meteorological Disaster Yearbook, edited by song Lianchun, China Meteorological Disaster Yearbook, meteorological publishing house, April 2018, Yearbook